Pergamon

0301-9322(94)E0004-3

Int. J. Multiphase Flow Vol. 20, No. 5, pp. 805–818, 1994

0301-9322/94 $7.00 + 0.00

PHASE DISTRIBUTION IN BUBBLY TWO-PHASE FLOW IN VERTICAL DUCTS

M. LOPEZ DE BERTODANO, R. T. LAHEY JR and O. C. JONES
Rensselaer Polytechnic Institute, Troy, NY 12180-3590, U.S.A.

(Received 10 August 1992; in revised form 13 January 1994)

Abstract—The lateral phase distribution in bubbly flows in vertical ducts was analyzed using a three-dimensional two-fluid model. The constitutive relations of the model are based on analytic and experimental information on the behavior of a single bubble, and on the assumption of linear superposition of shear-induced and bubble-induced turbulence.

The experiments chosen to test the model include available data for pipes and new data obtained in an isosceles triangular duct. While most of the data could be reproduced satisfactorily by the model, some could not. This is attributed to certain physical mechanisms that are still not well understood and therefore were not included in the constitutive relations.

Key Words: phase distribution, bubbly flows, two-fluid models

1. INTRODUCTION

The objective of this research was to advance the state-of-the-art in multidimensional two-phase CFD. In particular, to predict the lateral phase distribution for bubbly flows in ducts. One-dimensional two-phase flow methods have been widely used in the past for design calculations. The simplest was the homogeneous equilibrium mixture model (HEM). Such models have been upgraded by prescribing velocity and void distribution profiles, and the relative velocity between the phases. For example, the drift-flux model of Zuber & Findlay (1965). However, these models require *a priori* knowledge of the lateral distributions. Since these are not well known normally, it would be much better to perform multidimensional calculations with an appropriate two-fluid model. There are many applications in the power and chemical industries that could benefit from more accurate two-phase flow predictions. For example, the prediction of the local critical heat flux in the fuel rod bundles of nuclear reactors is an important calculation that normally determines the maximum allowable operating power. This calculation has been performed with subchannel computer codes such as COBRA (Wheeler *et al.* 1986) which compute quantities averaged across the subchannel area. The transport processes within these subchannels are accounted for using algebraic correlations. As computers become more and more powerful, it appears feasible to perform more detailed calculations within a subchannel, however in order to do so with accuracy it is necessary to better understand the physical mechanisms that occur at this smaller scale.

A rigorous development of the three-dimensional time averaged two-phase flow conservation equations has been given by Ishii (1975) and updated by Lahey & Drew (1990). The resultant model is called a two-fluid model. In addition to the Reynolds stresses, these conservation laws contain new interfacial transfer terms which result from the averaging process. Thus prior to numerically evaluating the two-fluid conservation equations, it is necessary to constitute the Reynolds stresses and the interfacial forces, such that closure is achieved.

One of the earlier works on turbulence modeling in conjunction with a multidimensional two-fluid model was published by Drew & Lahey (1982) who applied mixing length theory to analyze phase distribution in bubbly pipe flows. They were able to qualitatively predict the effect of wall peaking in upward bubbly flows and void coring for downflows. Thus, it was shown that turbulence could be a dominant mechanism in lateral phase distribution.

More elaborate computations of two-phase turbulence were performed by Lee *et al.* (1989) who adapted the k–ε model for bubbly flow. Lopez de Bertodano *et al.* (1990) extended this work to the τ–ε model to account for the effect of non-isotropy. However, at this time problems were

encountered with the low velocity flow computations (i.e. $j_L = 0.5$ m/s). Because of this a new way to constitute a k–ϵ model for bubbly flows has been proposed (Lopez de Bertodano 1992).

The effect of bubbles on the turbulent field is very important, since not only does the turbulence field in the liquid affect the distribution of bubbles, but the bubbles also affect the liquid phase's turbulence. Lance & Bataille (1991), who measured two-phase grid-generated turbulence and observed that for their data the kinetic energy of the single-phase grid-generated turbulence and the bubble-induced turbulence could be linearly superimposed. Theofanous & Sullivan (1982) made the same observation for their measurements at the centerline of a pipe at low liquid flow rates. However, Serizawa *et al.* (1986) and Wang *et al.* (1987), who measured the Reynolds stresses and phase distribution in bubbly pipe flows, have observed that at higher liquid velocities ($j_L \geqslant 1$ m/s) the turbulence level in the center region of the pipe can be lower than for single-phase, that is, turbulence suppression was observed. Lopez de Bertodano (1992) obtained turbulence data and phase distribution data for a triangular duct, in order to further demonstrate the multidimensional capabilities of the two-fluid model.

The other key issue in two-fluid CFD is the interfacial forces. The drag force on bubbles has been thoroughly investigated. Others like the virtual mass force and the lift force may be derived from first principles for inviscid flow (Drew & Lahey 1987, 1990). In particular, the lift force or any other force that acts in the lateral direction is very important to predict phase distribution. The behavior of these forces in viscous turbulent flows is not yet fully understood. However, Lance & Naciri (1991) performed an experiment in which they were able to measure lift on a bubble.

The two-fluid model will be presented first. Then the constituted relations will be discussed. Finally, comparisons between computations experimental data for pipes and a triangular duct will be shown.

2. MATHEMATICAL MODEL

2.1. Two-phase mass and momentum conservation equations

The Eulerian conservation equations for each phase may be averaged in various ways (i.e. time averaging, volume averaging, ensemble averaging). The result is known as the two-fluid model. For isothermal, incompatible gas–liquid flow without phase change, these averaged conservation equations are (Ishii 1975):

Conservation of mass

$$\frac{D_k}{Dt}\epsilon_k + \epsilon_k \nabla \cdot \bar{\mathbf{u}}_k = 0, \quad (k = \mathrm{L}, \mathrm{G}) \tag{1}$$

where, the material derivative of phase k is given by:

$$\frac{D_k}{Dt} = \frac{\partial}{\partial t} + \bar{\mathbf{u}}_k \cdot \nabla \tag{2}$$

and where the subscript k refers to the liquid or vapor phases, the overbars indicate time-averaged quantities, the bold characters indicate vector quantities, ϵ_k is the volume fraction of phase k, $\mathbf{u}_k$ is the corresponding velocity and D_k/Dt is the material derivative of phase k.

Conservation of momentum

$$\epsilon_k \rho_k \frac{D\bar{\mathbf{u}}_k}{Dt} = (\nabla \cdot \epsilon_k(\bar{\mathbf{T}}_k + \tau_k^{\mathrm{Re}}) + \rho_k \mathbf{g}) + \mathbf{M}_k \tag{3}$$

where, neglecting viscous stresses, the stress tensor for phase k is given by,

$$\bar{\mathbf{T}}_k + \tau_k^{\mathrm{Re}} = -\bar{p}_k \mathrm{I} - \rho_k \overline{\mathbf{u}_k' \mathbf{u}_k'} \tag{4}$$

and the instanteous velocity of phase k is:

$$\mathbf{u}_k = \bar{\mathbf{u}}_k + \mathbf{u}_k' \tag{5}$$

The phasic density is ρ_k (assumed constant), $\bar{p}_k$ is the static pressure, $\mathbf{g}$ is the gravitational acceleration, $\mathbf{M}_k$ is the net interfacial force on phase k, and the term $-\rho_k \overline{\mathbf{u}_k' \mathbf{u}_k'}$ is the Reynolds stress

tensor. In the vapor momentum equation the Reynolds stresses are small in comparison with the pressure gradient and the interfacial forces, so they can be neglected. This assumption is good for low pressure air–water flows where the vapor density is relatively small. Hence, from here on, the subscript k in the term $\overline{\mathbf{u}_k'\mathbf{u}_k'}$ will be dropped with the understanding that this term corresponds to the liquid phase.

The interfacial jump condition, neglecting surface tension, is:

$$\mathbf{M}_G + \mathbf{M}_L = 0 \qquad [6]$$

In order to have a working two-fluid model it is necessary to constitute the interfacial forces and the Reynolds stress tensor, $\mathbf{u}_L'\mathbf{u}_L'$, for turbulent bubbly flow.

2.2. Constitutive relations for interfacial momentum transfer

The interfacial force is customarily divided into several components, for example: drag, virtual mass, lift and the averaged interfacial pressure term:

$$M_L = M_L^D + M_L^{vm} + M_L^L + M_L^P \qquad [7]$$

Of all these, the drag force has been the most thoroughly investigated. The axial drag force per unit volume is given by:

$$\mathbf{M}_L^D = \tfrac{3}{4} C_D \frac{\rho_L}{D_b} \epsilon_G |\bar{\mathbf{u}}_R| \bar{\mathbf{u}}_R \qquad [8]$$

where

$$\bar{\mathbf{u}}_R = \bar{\mathbf{u}}_G - \bar{\mathbf{u}}_L,$$

D_b is the bubble diameter and C_D is the drag coefficient of the bubbles for which many correlations are available.

The virtual mass force is expressed as:

$$\mathbf{M}_L^{vm} = C_{vm} \epsilon_G \rho_L \left(\frac{D_G}{Dt} u_G - \frac{D_L}{Dt} u_L \right) \qquad [9]$$

where C_{vm} is the virtual mass coefficient which represents the inertia of the bubble-induced fluid flow. For potential flow around a sphere moving in helical paths potential flow theory and measurements (Lance & Bataille 1991) indicate that C_{vm} may be considerably higher, i.e.

$$1.2 < C_{vm} < 3.4 \qquad [10]$$

for 5 mm air bubbles rising in water.

The lift force obtained from inviscid rotational flow theory is:

$$M_L^L = C_L \epsilon_G \rho_L \bar{\mathbf{u}}_R \times \nabla \times \bar{\mathbf{u}}_L \qquad [11]$$

where $C_L = 1/2$ for flow around spheres and more generally $C_L = C_{vm}$ for other geometries. The experiment performed at the Ecole Centrale de Lyon by Lance & Naciri (1991) for single bubbles in a rotating tank indicate that $C_L \cong 1/4$ for a wide range of sizes smaller than Taylor bubble sizes.

Near a wall the velocity distribution around the bubble changes so the lift force is expected to vary. To account for this Antal *et al.* (1991) has proposed a wall lift force:

$$M_L^W = \left(C_{w1} + C_{w2} \frac{R_b}{y} \right) \epsilon_G \rho_L \frac{|\bar{\mathbf{u}}_R|^2}{R_b} \mathbf{n}_w \qquad [12]$$

where R_b is the bubble radius, $\mathbf{n}_w$ is the outward normal to the wall and y is the distance from the wall. In order to find values for the coefficients Kurul (1991) performed CFD calculations of a sphere close to a wall and obtained $C_{w1} = -0.1$ and $C_{w2} = 0.147$. This lubrication-like lift force arises in the thin layer between the bubble and the wall. In contrast, the lift force discussed previously is caused by inertia and is based on potential flow theory. It is possible that a viscous lift force is also present, however for the type of bubbles of interest (i.e. $Re_b \cong 1000$) inertia predominates. Given the complexity of the phenomenon, the simplest theory was used as long as it captured the relevant physics.

Both the turbulence and the relative velocity affect the instantaneous pressure at the interface. The effect of turbulence is not properly understood yet. The effect of the average relative velocity on the other hand is clearer. The simplest possible case is for potential flow around a sphere (Lamb 1932):

$$\bar{p}_{Li} = \bar{p}_L - C_p \epsilon_G \rho_L |\bar{u}_R|^2 \quad [13]$$

which is used to constitute the interfacial pressure term:

$$M_L^P = -\bar{p}_{Li} \nabla \alpha_L = (\bar{p}_{Li} - \bar{p}_L) \nabla \epsilon_L + \bar{p}_L \nabla \epsilon_L \quad [14]$$

where the pressure coefficient, C_p is 0.25 for non-interacting spherical bubbles. If the bubble is not spherical, then $C_p > 0.25$. In the case of a wake behind the bubble, the flow is practically potential until the point where separation occurs. Since the pressure at the rear cannot recover up to the stagnation value (which is higher than the liquid average pressure), the pressure averaged over the interface must be lower than for potential flow, and so again, $C_p > 0.25$.

Real bubbles are a combination of these effects, so values of C_p significantly greater than 1/4 may be expected. For example, using the data of Lance & Bataille (1991) for the shape and trajectory of 5 mm oblate spheroid bubbles moving in helical paths in water, and the potential flow analysis of Saffman (1956) it may be shown:

$$0.5 < C_p < 0.7 \quad [15]$$

If the effect of a wake is considered these numbers should be even bigger. Unfortunately there is no accurate way to account for the effect of a wake on the pressure distribution around a bubble (Fan & Tsuchiya 1990).

2.3. Constitutive relations for the Reynolds stresses

The key assumption made to model the two-phase bubbly flow turbulence in the liquid phase is that the shear-induced turbulence and the bubble-induced turbulence are weakly coupled. Therefore they can be superposed linearly. This approximation is expected to be most valid for dilute bubbly flows. Thus the Reynolds stress tensor for the continuous liquid phase may be written as:

$$\tau_L^{Re} = \tau_{L(BI)}^{Re} + \tau_{L(SI)}^{Re} \quad [16]$$

The bubble-induced turbulence is calculated from the potential flow around a single bubble (Nigmatulin 1979). The general form for $\tau_{L(BI)}^{Re}$ is given by:

$$\tau_{L(BI)}^{Re} = 2\mathbf{A}_{(BI)} k_{L(BI)} \quad [17]$$

where $k_{L(BI)}$ is the kinematic energy associated with the perturbation of the liquid flow induced by the bubbles and $\mathbf{A}_{(BI)}$ is the anisotropy matrix, which is a function of the shape and the trajectory of the bubbles.

For the bubble-induced turbulence, the anisotropy matrix for potential flow around a sphere was used, i.e.:

$$\mathbf{A}_{(BI)} = \begin{pmatrix} 4/10 & 0 & 0 \\ 0 & 3/10 & 0 \\ 0 & 0 & 3/10 \end{pmatrix} \quad [18]$$

The shear-induced part is written as:

$$\tau_{L(SI)}^{Re} = \nu_L^t (\nabla \bar{\mathbf{u}}_L + \nabla \bar{\mathbf{u}}_L^T) + 2\mathbf{A}_{(SI)} k_{L(SI)} \quad [19]$$

where ν_L^t is the turbulent viscosity in the liquid, $k_{L(SI)}$ is the turbulent kinetic energy associated with the shear-induced turbulence and $\mathbf{A}_{(SI)}$ is an anisotropy matrix for the shear-induced turbulence. In the calculations performed for the triangular duct, the anisotropy of the turbulence had to be taken into account in order to capture the recirculating flows. This can be achieved by using the τ–ε model (Lopez de Bertodano *et al.* 1989). Due to the early stage of development of the two-fluid model a simpler algebraic stress model (Naot & Rodi 1982) was adopted here.

The modeling of $k_{L(SI)}$ used is based on the standard k–ε model (Launder & Spalding 1976), i.e.

$$\epsilon_L \frac{D_L}{Dt} k_{L(SI)} = \nabla \cdot \epsilon_L (\nu_L^t \nabla k_{L(SI)}) + (P_L - \varepsilon_L) \quad [20]$$

where the turbulent dissipation rate ε_L is given by:

$$\epsilon_L \frac{D_L \varepsilon_L}{Dt} = \nabla \cdot \epsilon_L \left(\frac{\nu_L^t}{\sigma_\varepsilon} \nabla \varepsilon_L \right) + \epsilon_L \left(C_{\varepsilon 1} \frac{\varepsilon_L P_L}{k_{L(SI)}} - C_{\varepsilon 2} \frac{\varepsilon_L^2}{k_{L(SI)}} \right) \quad [21]$$

and P_L is the turbulence production rate:

$$P_L = \nu_L^t (\nabla \bar{\mathbf{u}}_L + \nabla \bar{\mathbf{u}}_L^T) : \nabla \mathbf{u}_L . \quad [22]$$

The constants $C_{\varepsilon 1}, C_{\varepsilon 2}, \sigma_\varepsilon$ are specified as in the standard single-phase flow k–ε model: $\sigma_\varepsilon = 1.3$, $C_{\varepsilon 1} = 1.44$, $C_{\varepsilon 2} = 1.92$.

Lopez de Bertodano (1992) introduced an additional transport equation for the bubble-induced turbulent kinetic energy:

$$\epsilon_L \frac{D_L}{Dt} k_{L(BI)} = \nabla \cdot \epsilon_L (\nu_L^t \nabla k_{L(BI)}) + \frac{1}{\tau_{BI}} (k_{L(BI)_a} - k_{L(BI)}) \quad [23]$$

where $k_{L(BI)_a}$ is the asymptotic value corresponding to the kinetic energy brought to the liquid by bubbles rising at their terminal velocity. Here, τ_{BI} is the bubble relaxation time:

$$\tau_{BI} = 2R_b / u_T \quad [24]$$

R_b and u_T standing respectively for bubble mean radius and terminal velocity.

In most practical situations, τ_{BI} is very small, so that the equation for the bubble-induced turbulence reduces to $k_{L(BI)} = k_{L(BI)_a}$, which is the equation used by Lance & Bataille (1991).

According to potential flow theory:

$$k_{L(BI)_a} = \tfrac{1}{2} \epsilon_G \rho_L C_{VM} |\bar{\mathbf{u}}_R|^2 \quad [25]$$

The experimental value obtained for C_{VM} independently by Lopez de Bertodano (1992) and Lance & Bataille (1991) was approx. 2, which lies between the theoretical limits prescribed by [10].

In the single-phase k–ε model, the turbulent viscosity is expressed by:

$$\nu_L^t = C_\mu \frac{k_{L(SI)}^2}{\varepsilon_L} \quad [26]$$

where $C_\mu = 0.09$ (Rodi 1984). Sato (1981) proposed to calculate two-phase viscosity by linear superposition of the shear-induced and bubble-induced turbulent viscosities, which, for a k–ε model, leads to:

$$\nu_L^t = C_\mu \frac{k_{L(SI)}^2}{\varepsilon_L} + C_{\mu b} R_b \epsilon_G |\mathbf{v}_r| \quad [27]$$

with $C_{\mu b} = 1.2$. This is equivalent to adding the shear stresses and is thus fully compatible with [16].

The turbulence in the dispersed gaseous phase may be neglected provided that $\rho_G \ll \rho_L$. Then the stress tensor given in [4] simplifies to

$$T_G = -p_{Gi} I = -p_{Li} I \quad [28]$$

neglecting the effect of surface tension.

2.4. Interfacial structure

The most important shortcoming of the current two-fluid model is that it cannot predict the interfacial structure (e.g. the bubble size distribution); rather, the mean bubble size is an input. Moreover, the model is only valid for monodispersed bubbles. However, a multigroup model could be devised by adding a set of interacting conservation equations for each bubble size group. Then different constitutive relations could be applied, as necessary, to these groups.

2.5. Boundary conditions

From a physical point of view the correct velocity boundary conditions for steady flow in ducts are:

(i) for the liquid phase the distribution at the inlet and the no slip condition at the walls.
(ii) for the gaseous phase the condition at the walls depends on whether or not the viscous term is retained in the momentum equations. If not, then the "no slip" condition must be replaced by the potential flow boundary condition (i.e. zero velocity normal to the wall).

For the void fraction, $\epsilon_G = 1 - \epsilon_L$, the distribution at the inlet is sufficient. This may be explained in terms of the continuity equation of the gaseous phase, [1]: in principle, given the velocity field, it may be solved for the void fraction along the characteristics which start at the duct inlet.

If a numerical solution is performed, it is impractical to use the no slip condition because the necessary mesh size would be too small. Instead the velocity tangential to the wall is specified at some distance away from the wall as in single-phase turbulent flow, i.e. the logarithmic law of the wall is used in the buffer zone.

Marié found that for bubbly flow the law of the wall is still valid but is slightly shifted. The present data indicate that the slope changes too (see figure 1). Nevertheless, for simplicity, in this study the single-phase logarithmic law was used as the liquid momentum boundary condition:

$$\frac{\bar{u}_L}{u_*} = \frac{1}{k} \ln y_+ + b \qquad [29]$$

where

$$u_* = \sqrt{\frac{\tau_w}{\rho_L}}, \quad y_+ = \frac{y \bar{u}_L}{u_L}, \qquad [30]$$

$\kappa = 0.435$ and $b = 5.4$. The Reynolds stress boundary conditions are given by Launder *et al.* (1975):

$$\overline{\mathbf{u}'_L \mathbf{u}'_L} = \begin{pmatrix} 5.1 & 0 & 1.0 \\ 0 & 2.3 & 0 \\ 1.0 & 0 & 1.0 \end{pmatrix} u_*^2 \qquad [31]$$

so the kinetic energy is obtained from the trace of this equation:

$$k_L = 4.2 u_*^2 \qquad [32]$$

Finally, the dissipation boundary condition is also given by Launder *et al.* (1975):

$$\varepsilon_L = \frac{u_*^3}{\kappa y} \qquad [33]$$

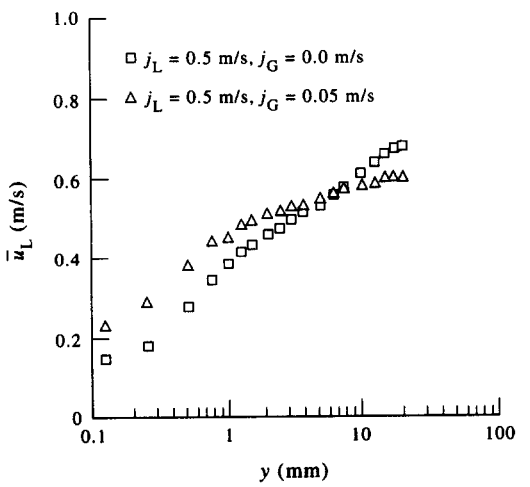

Figure 1. Boundary layer velocity measurements for single-phase and two-phase flow, logarithmic scale.

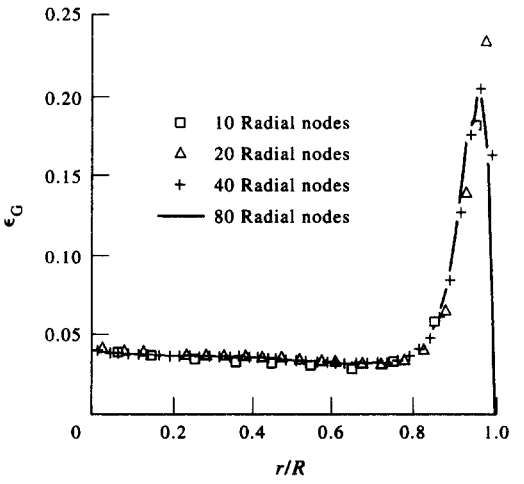

Figure 2. Effect of radial mesh refinement on void distribution.

This set of constitutive equations and boundary conditions is not completely definitive. However, it does contain all the relevant mechanisms that have an effect on the motion of the bubbles at low liquid flow rates. On the other hand, at high liquid flow rates there appear to be other mechanisms that are not included. For example, the diffusion of the bubbles by the shear induced-turbulence field. Relatively simple constitutive relations were chosen in this study. As modeling uncertainties are resolved the advantage of more elaborate constitutive relations should become more clear.

3. RESULTS

3.1. Numerical method

The two-fluid model closure laws were implemented into the PHOENICS code (Spalding & Norton 1987). For the case of steady state fully developed duct flows an efficient computational strategy is to neglect axial diffusion so the problem becomes parabolic with axial distance as the time-like variable. This works provided that there is no flow reversal. Then a marching method can be used starting at the inlet and the flow variables evolve similarly to the developing flow in a duct. The similarity is not complete because axial diffusion has been neglected, but once fully developed flow is attained this difference does not matter.

The appropriate boundary conditions at the inlet and at the walls have beeen discussed already. For the parabolic scheme no boundary conditions are necessary at the outlet.

Mesh refinement tests were carried out for the pipe computations. Results of the effect of mesh size on void distribution for a particular case are shown in figure 2.

3.2. Flow in pipes

There is a considerable amount of bubbly two-phase flow experimental data in pipes. High amplitude void peaks near the wall have been observed in many cases. Among these the data of Serizawa *et al.* (1986) and Wang *et al.* (1987) are particularly useful since they include Reynolds stress measuremnts performed with multiple-sensor hot film anemometers. Comparisons of computations and data for these and other cases follow.

Figures 3 to 6 show a comparison with Serizawa's data for $j_L = 1.36$ m/s and $j_G = 0.077$ m/s. The pipe diameter was 2 in. and the length-to-diameter ratio was $L/D = 43$. The amplitude of the wall void fraction peak was matched with $C_L = 0.1$ (see figure 3). The bubble-induced turbulence, which was the dominant component of the turbulence at the center-line, was predicted with $C_{VM} = 2.0$ (see figure 5). In accordance with the result for potential flow around a sphere the pressure coefficient was set to $C_p = \frac{1}{2} C_{VM}$. This is an interesting case because the two-phase turbulence intensity is lower than the corresponding single-phase intensity, which may be explained in terms

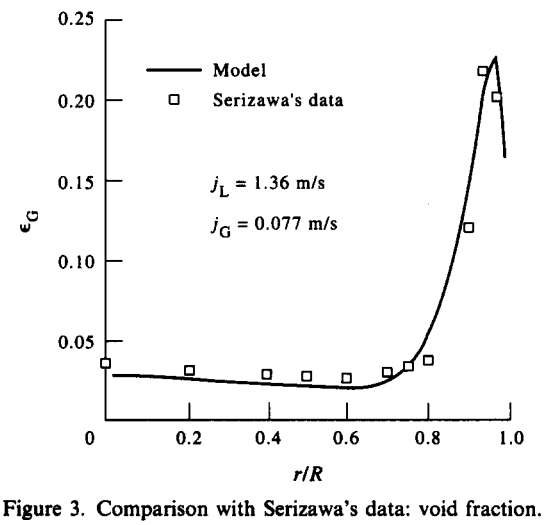

Figure 3. Comparison with Serizawa's data: void fraction.

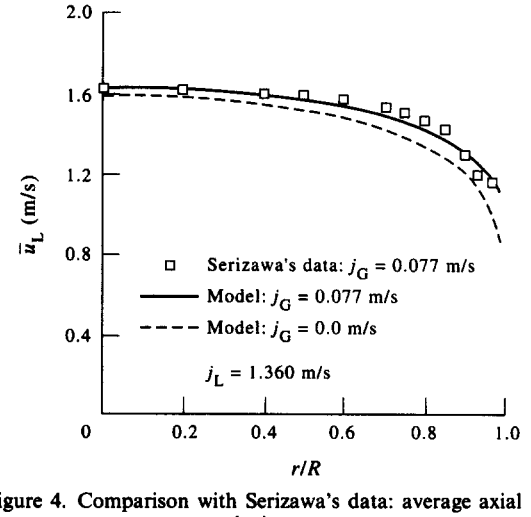

Figure 4. Comparison with Serizawa's data: average axial velocity.

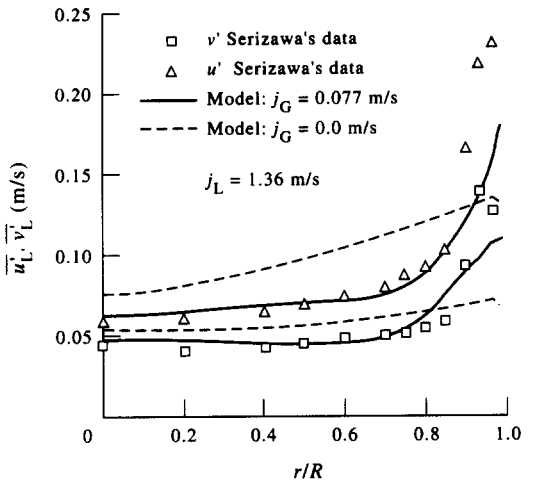

Figure 5. Comparison with Serizawa's data: velocity fluctuations.

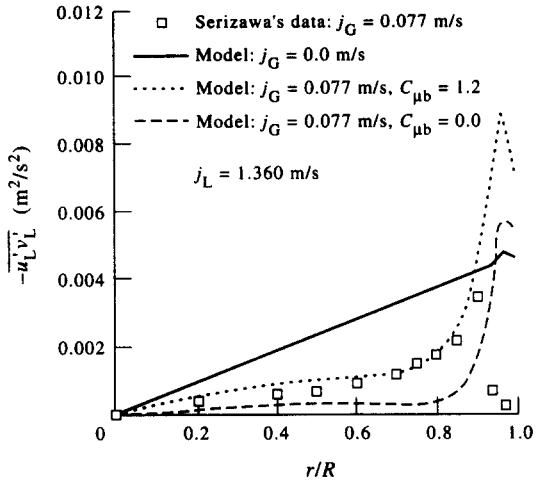

Figure 6. Comparison with Serizawa's data: shear stress.

of figures 4 and 6. From these figures it is seen that for two-phase flow the velocity profile is flatter and the shear stress is lower so the production of shear-induced turbulence, $P_L = -\overline{u'v'}\partial\bar{u}_L/\partial r$, is significantly reduced and the contribution of bubble-induced turbulence cannot make up the difference. Figure 6 also shows the effect of Sato's model for bubble-induced viscosity on the computed shear stress.

The same values of C_L, C_{VM} and C_p were used in the comparisons with Wang's data. Figure 7 shows a downflow case with $j_L = 1.08$ m/s and $j_G = 0.1$ m/s. The pipe diameter was 2 in. and $L/D = 40$. Since the effect of turbulence is to create a gradient that pushes the bubbles toward the wall this case is further evidence that an additional lateral force (i.e. lift) is at work.

Figures 8–12 show comparisons with two cases of Wang's upflow data: $j_L = 1.08$ m/s with $j_G = 0.10$ and 0.40 m/s. The latter is a high void fraction case well beyond the domain of validity of the assumption of weak coupling between shear-induced and bubble-induced turbulence. Nevertheless, the results of the model are quite good. In particular, the void fraction distribution (figure 8), is reproduced well. For the normal Reynolds stresses at $j_G = 0.40$ m/s (figure 11), a lower value of the virtual mass coefficient had to be used, i.e. $C_{vm} = 2C_p = 1.2$, which is the lower bound given by [11]. This is an indication that for high void fractions the bubble-to-bubble non-linear interactions affect the bubble-induced turbulence. Also the non-isotropy predicted by the model is less than the measured non-isotropy. The comparison with the shear stress data (figure 12) is not good. Wang's shear stress data looks different from the data of Serizawa *et al.* (1986) and Lopez

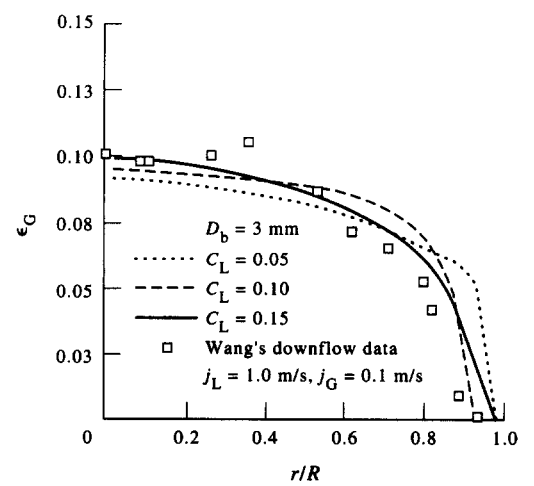

Figure 7. Comparison with Wang's downflow data: void fraction.

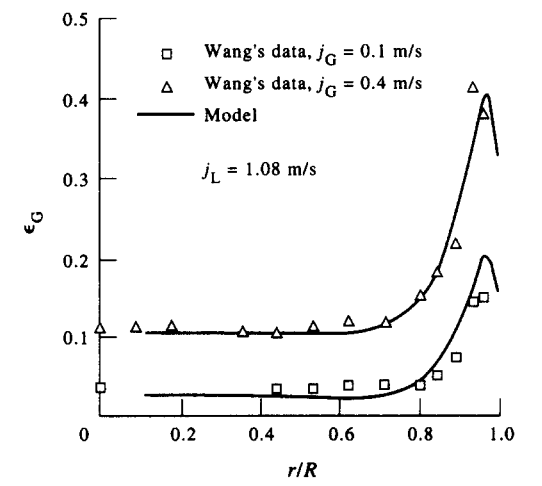

Figure 8. Comparison with Wang's upflow data: void fraction.

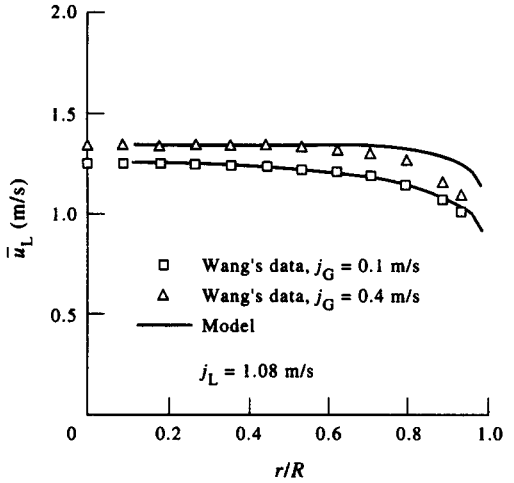

Figure 9. Comparison with Wang's upflow data: average axial velocity.

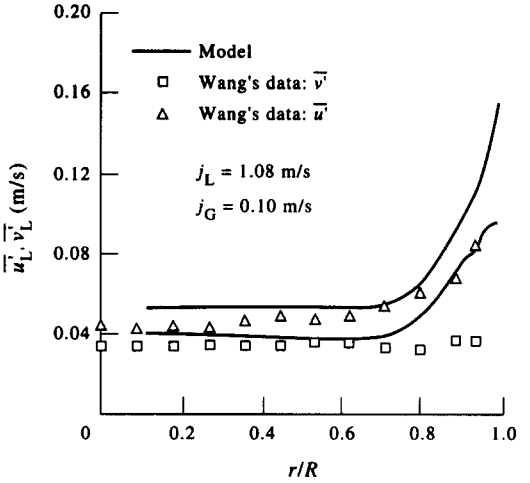

Figure 10. Comparison with Wang's upflow data (1987): velocity fluctuations, $j_G = 0.1$ m/s.

de Bertodano *et al.* (1992). The latter two used X-sensor probes which are specifically designed for this purpose whereas Wang used a three-sensor conical probe. The discrepancies shown in figure 12 may be caused to some extent by this.

Not all comparisons with void fraction data are successful. Recent data by Liu (1991) clearly indicate the effect of bubble size on phase distribution which the present closure laws do not consider. Comparisons are shown on figure 13 for $j_G = 0.2$ m/s. The pipe diameter is 2 in. and measurements were made at $L/D = 30$, 60, 90 and 120. Below $L/D = 120$ the two-fluid model can predict the void peak. But at $L/D = 120$ the void peak practically disappears and the only way to match its amplitude is to reduce the lift coefficient to $C_L = 0.02$. Apparently the growth of the bubbles, as the hydrostatic head decreases and coalescence takes place along the pipe results in a significant change in the lateral lift force.

The sensitivity of the model to the coefficients of the constitutive relations and other model parameters may be significant. Figure 14 shows the effect of the lift coefficient. It is clear that for this case lateral lift is dominant compared to turbulence effects. At higher velocities turbulent diffusion plays an important role and the void peak decreases.

Figure 15 shows the sensitivity of the void distribution to bubble size. In this model the effect of bubble size is only limited to the wall force. In fact, this is the only constitutive relation in which it appears explicitly. It could also affect the lift force and the interfacial pressure force if the relative

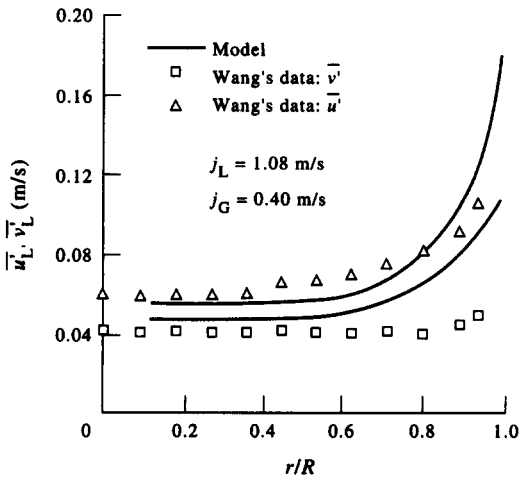

Figure 11. Comparison with Wang's upflow data: velocity fluctuations, $j_G = 0.40$ m/s.

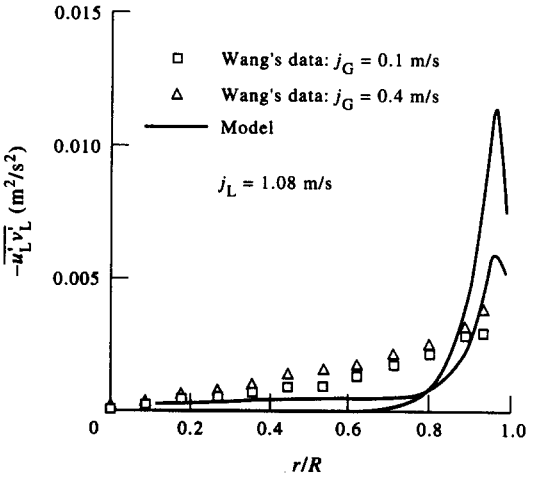

Figure 12. Comparison with Wang's upflow data: shear stress.

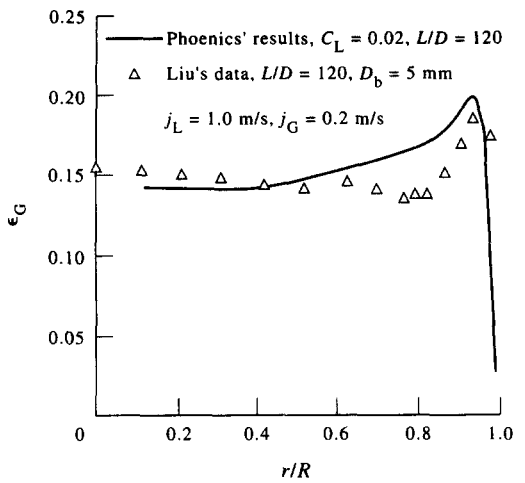

Figure 13. Comparison with Liu's data: void fraction.

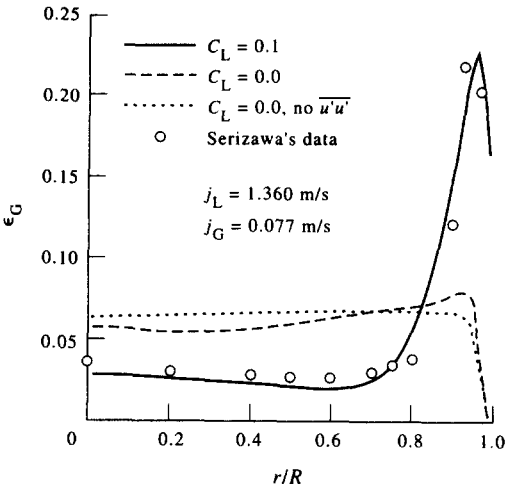

Figure 14. Effect of lift coefficient and Reynolds stresses on phase distribution.

velocity, or the shape of the bubble, were to change. However, the rise velocity of bubbles between 2 and 10 mm in diameter is practically constant and the bubble shape does not influence model prediction unless the value of the closure coefficients are changed.

Figure 16 shows the effect of the interfacial pressure coefficient, C_p. The interfacial pressure force acts like a diffusive force. The physical interpretation is that the pseudo-turbulence and the wake-induced turbulence of a bubble affect the trajectory of the surrounding bubbles. The important thing is that these coefficients have physical meaning and they can be assigned proper values in terms of mechanistic arguments.

3.3. *Flow in a triangular duct*

Lopez de Bertodano (1992) obtained bubbly upflow data in a triangular duct with 2 in. base, 4 in. height and $L/D = 70$. The liquid velocities were 0.5 and 1.0 m/s. He used an X-sensor hot film probe to measure Reynolds stresses. The purpose of the experiment was to obtain data to test the two-fluid model in a nonaxisymmetric geometry.

Comparisons between the model and data for $j_L = 1.0$ m/s and $j_G = 0.1$ m/s and $j_G = 0.6$ m/s are shown in figures 17–21. These computations were performed with the same values of C_L, C_{vm} and C_p used for the pipe calculations. In particular, $C_{vm} = 2.0$ was used for the low void fraction

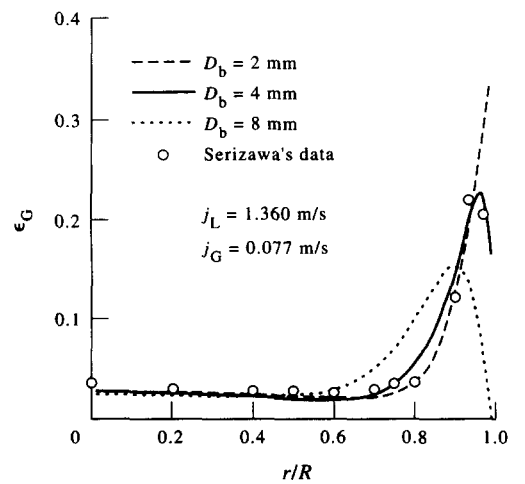

Figure 15. Effect of bubble size on phase distribution.

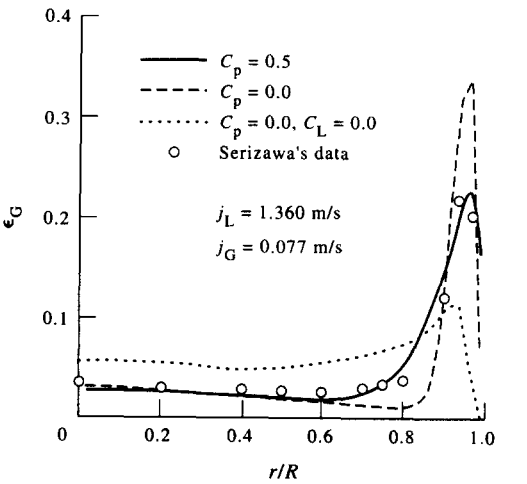

Figure 16. Effect of pressure coefficient on phase distribution.

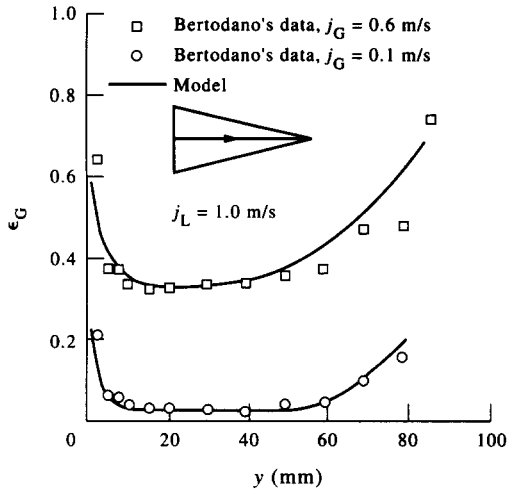

Figure 17. Comparison with Lopez de Bertodano's data: void fraction.

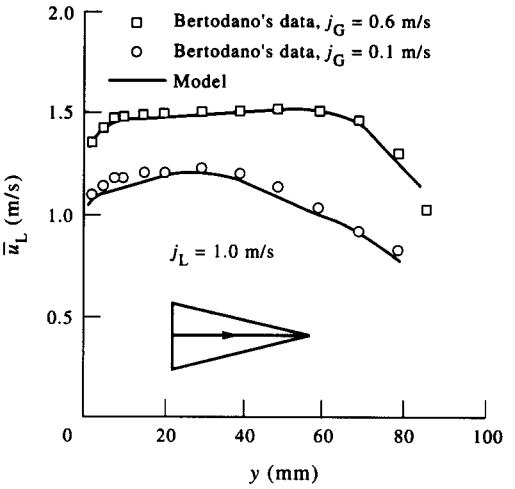

Figure 18. Comparison with Lopez de Bertodano's data: average axial velocity.

calcuations and $C_{vm} = 1.2$ was used for high void fraction cases. In general, the model predictions for void fraction and velocity agree with the data.

The computed shear stress with and without Sato's model is shown in figure 21. The benefit of including the two-phase viscosity is not as clear as in the case of Serizawa's pipe data (figure 6).

The effect of recirculating flows on void distribution was investigated. This was the reason to introduce anisotropy in the turbulence model. Figures 22 and 23 show the model results for the recirculation in single-phase and two-phase flows. The presence of the bubbles causes a reduction in the lateral turbulence gradient so the lateral pressure gradient and consequently the recirculating velocities must decrease.

4. CONCLUSION

A two-fluid formulation of two-phase flows has been used to numerically predict bubbly flows in two different situations (a pipe, and a triangular duct). The obvious conclusion to be drawn from these numerical simulations is that proper mechanistic closure laws lead to realistic predicitons for the geometries adopted here. The CFD code used for single-phase flow proved to be able to deal with the equations of the two-fluid model, at least for simple situations. The closure laws were obtained from basic fluid dynamic analysis of the flow around a single bubble. The shear-induced

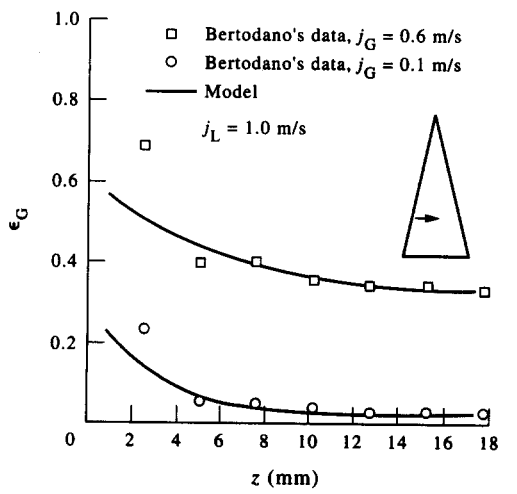

Figure 19. Comparison with Lopez de Bertodano's data: void fraction.

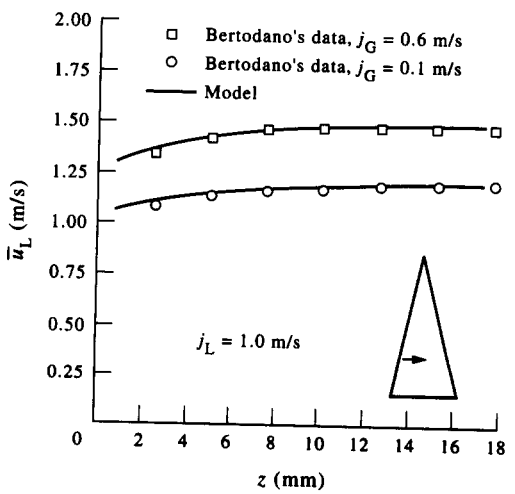

Figure 20. Comparison with Lopez de Bertodano's data: average axial velocity.

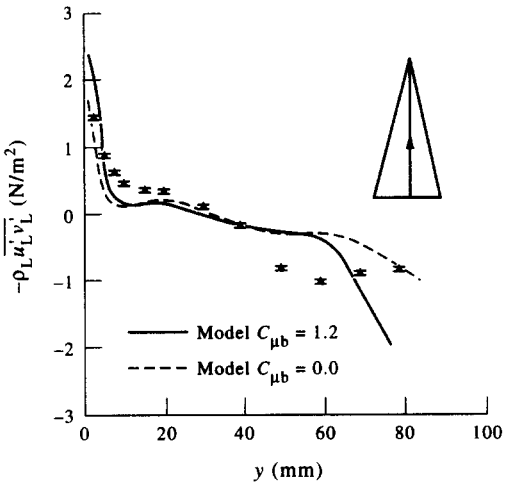

Figure 21. Comparison with Lopez de Bertodano's data: shear stress.

turbulence was calculated using the well-known k–ε model for single-phase flows. Therefore, the number of adjustable parameters were limited, and these can be related to measurable quantities, such as the virtual mass coefficient and the lift coefficient. It is worth noting that, although these closure hypotheses were expected to be restricted to low void fraction, reasonable agreements with

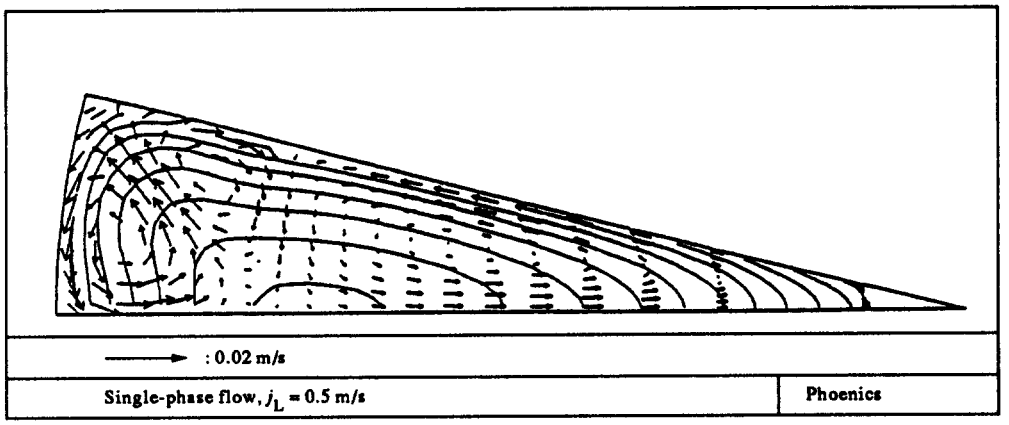

Figure 22. Single-phase flow computations for the triangle: vector plot of the recirculating flows and contour plot of the axial velocity.

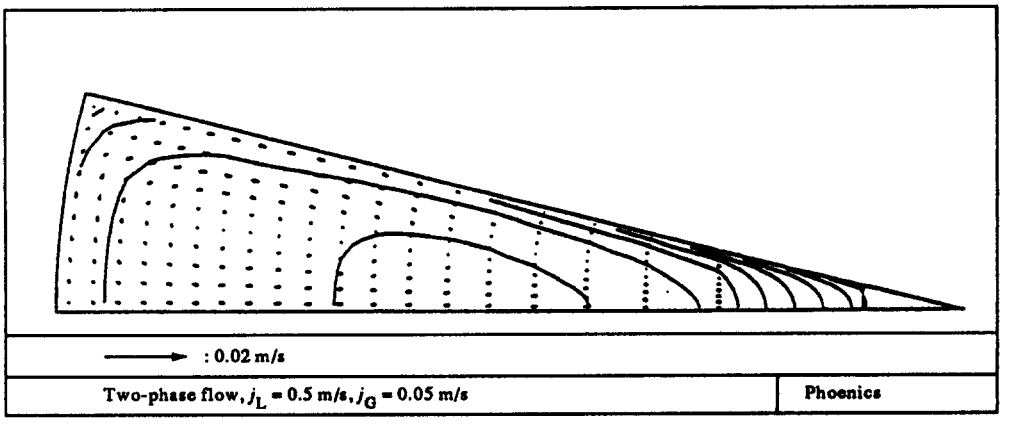

Figure 23. Two-phase flow computations for the triangle: vector plot of the recirculating flows and contour plot of the axial velocity.

experiment were achieved for high void fraction bubbly flows. Nevertheless, these calculations indicate that a better understanding of basic mechanisms is still required.

(a) *Turbulence*
The turbulence models which have been tested here are based on linear superposition, the assumption that the coupling between shear-induced and bubble-induced fluctuations is weak, which is likely not the case for high void fraction. Unfortunately, non-linear coupling has not yet been modeled.

(b) *Interfacial momentum transfer*
The nature of the interfacial force is not well understood. For the lift coefficient, a value of 0.1 resulted in good comparisons with most of the data. However, a value of 0.02 was necessary to match the low amplitude void fraction peak measured by Liu at $L/D = 120$. This result may be due to an effect of the bubble size on the mechanism of lift, although this process is not well understood. Moreover, at present it is still impossible to predict the evolution of the size distribution of a population of bubbles under the effect of turbulence, interfacial forces and mutual interactions. Furthermore, the effect of turbulence on lift, as well as on the other forces, is not clear either.

The interfacial force near a wall is another topic which requires further studies.

(c) *Boundary conditions*
The choice of appropriate boundary conditions is crucial in many problems. In particular, when transport phenomena at the wall are of interest. The experiments by Marié (1987) show that a modified law of the wall can be adopted for low void fraction without phase change. However, this might not be true as the void fraction increases, due to the existence of a second length scale imposed by the bubble size. The extension of the two-fluid model to boiling bubbly flows requires a detailed investigation of the structure of the boundary layer when the bubbles are produced at the wall.

Even though the problems pointed out above have yet to be solved, significant progress has been achieved during the last few years in the prediction of phase distribution for bubbly flows. Multidimensional CFD for two-phase bubbly flows is beginning to look feasible.

Acknowledgements—The authors wish to gratefully acknowledge the support given by the NSF, which provided the funding for the triangular duct experiment and computer time at the NCSA CRAY-YMP, and also the comments of Dr Michel Lance which have been included in this paper.

REFERENCES

ANTAL, S. P., LAHEY, R. T. JR & FLAHERTY, J. E. 1991 Analysis of phase distribution in fully developed laminar bubbly two-phase flow. *Int. J. Multiphase Flow* **17,** 635–652.

DREW, D. & LAHEY, R. T. JR 1981 Phase distribution mechanisms in turbulent two-phase flow in channels of arbitrary cross section. *J. Fluid Engng* **203,** 583–589.

DREW, D. & LAHEY, R. T. JR 1982 Phase distribution mechanisms in turbulent two-phase flow in a circular pipe. *J. Fluid Mech.* **117,** 91–106.

DREW, D. & LAHEY, R. T. JR 1987 The virtual mass and lift force on a sphere in rotating and straining flow. *Int. J. Multiphase Flow* **13,** 113–121.

DREW, D. & LAHEY, R. T. JR 1990 Some supplemental analysis concerning the virtual mass and lift force on a sphere in a rotating and straining flow. *Int. J. Multiphase Flow* **16,** 1127–1130.

FAN, L.-S. & TSUCHIYA, K. 1990 *Bubble Wake Dynamics in Liquids and Liquid–Solid Suspensions.* Butterworth–Heinemann, Stoneham, MA.

ISHII, M. 1975 *Thermo-fluid Dynamic Theory of Two-phase Flow.* Eyrolles.

LAHEY, R. T. JR & DREW, D. A. 1990 The current state-of-the-art in the modeling of vapor/liquid two-phase flow. ASME Reprint, 90-WA/HT-13.

LAMB, H. 1932 *Hydrodynamics.* Dover, New York.

LANCE, M. & BATTAILE, J. 1991 Turbulence in the liquid phase of a uniform bubbly air–water flow. *J. Fluid Mech.* **22,** 95–118.

LANCE, M. & NACIRI, A. 1991 Lift and added mass coefficient for a single bubble. *First European Fluid Mechanics Conference*, September 1991, Cambridge, U.K.

LAUNDER, B. E., REECE, G. J. & RODI, W. 1975 Progress in the development of a Reynolds stress turbulence closure. *J. Fluid Mech.* **68,** 537–566.

LAUNDER, B. E. & SPALDING, D. B. 1974 The numerical computation of turbulent flows. *Comput. Meth. Appl. Mech. Engng* **3,** 269–289.

LEE, S.-J., LAHEY, R. T. JR & JONES, O. C. JR 1989 The prediction of two-phase turbulence and phase distribution phenomena using a K–ϵ model. *Jap. J. Multiphase Flow* **3,** 335–368.

LIU, T. J. 1991 The effect of bubble size on void fraction distribution in a vertical channel. *Proceedings of the International Conference on Multiphase Flows '91—Tsukuba* **1,** 453–457.

LOPEZ DE BERTODANO, M. 1992 Turbulent bubbly two-phase flow in a triangular duct. Ph.D. thesis, Rensselaer Polytechnic Institute, Troy, NY.

LOPEZ DE BERTODANO, M. LEE, S.-J., LAHEY, R. T. JR & DREW, D. A. 1990 The prediction of two-phase turbulence and phase distribution using a Reynolds stress model. *J. Fluids Engng* **112,** 107–113.

MARIÉ, J. L. 1987 Modeling of the skin friction and heat transfer in turbulent two-component bubbly flow in pipes. *J. Multiphase Flow* **113,** 309–325.

NAOT, D. & RODI, W. 1982 Calculation of secondary currents in channel flow. *Proc. Am. Soc. Civ. Engrs* **108,** (HY8) 948–968.

NIGMATULIN, R. I. 1979 Spatial averaging in the mechanics of heterogeneous and dispersed systems. *Int. J. Multiphase Flow* **5,** 353.

SATO, Y., SADATOMI, M. & SEKOGUCHI, K. 1981 Momentum and heat transfer in two-phase bubbly flow—I. *Int. J. Multiphase Flow* **7.**

SERIZAWA, A., KATAOKA, I. & MICHIYOSHI, I. 1986 Phase distribution in bubbly flow. *Proceedings of the Second International Workshop on Two-Phase Flow Fundamentals*, Data Set No. 24.

SPALDING, D. B. & ROSTEN, H. I. 1987 *The PHOENICS Reference Manual, CHAM/TR200, Document Version 06, Software Version 1.4.* CHAM Ltd, Wimbledon, England.

THEOFANOUS, T. G. & SULLIVAN, J. 1982 Turbulence in two-phase dispersed flows. *J. Fluid Mech.* **116,** 343–362.

WANG, S. K., LEE, S. J., JONES, O. C. JR & LAHEY, R. T. JR 1987 3-D turbulence structure and phase distribution measurements in bubbly two-phase flows. *Int. J. Multiphase Flow* **13,** 327–343.

WHEELER, C. L. *et al.* 1986 COBRA-NC: a thermal-hydraulic code of transient analysis of nuclear reactor components: equations and constitutive models. NUREG/CCR-3262..

ZUBER, N. & FINDLAY, J. A. 1965 Average volumetric concentration in two-phase flow systems. *J. Heat Transfer* 453–468.